Polymer(Korea) Vol. 22, No. 4, pp 659-669(1998)

Multi-fiber Fragmentation시험법을 이용한 Regular 및 Gradual Multi-fiber Composites의 계면특성

박종만† · 이상일 · 김진원 · 김대식

경상대학교 고분자공학과, 항공기부품기술연구센타

(1998년 3월 25일 접수)

A Study on Interfacial Properties of Regular and Gradual Multi-fiber Composites by Multi-fiber Fragmentation Test

Joung-Man Park†, Sang-Il Lee, Jin-Won Kim, and Dae-Sik Kim

Department of Polymer Science & Engineering, Regional Research Center for Aircraft Part Technology, Gyeongsang National University, Chinju 660-701, Korea

†e-mail : jmpark@nongae.gsnu.ac.kr

(Received March 25, 1998)

요 약: 섬유간의 간격에 의존하는 계면의 특성을 조사하기 위하여 두 형태의 복합재료 모델을 사용하였다. 하나는 균일간격이고, 다른 하나는 단계적 다섬유 복합재료이다. 다섬유 fragmentation시험법이 계면전단강도를 측정하기 위해 사용되었다. Weibull 통계에 의해, 유리섬유의 인장강도와 연신율은 size효과에 의해 게이지 길이가 증가함에 따라 감소하였다. 규칙 및 단계적 다섬유 복합재료로 부터는, 섬유간 간격이 증가함에 따라, 섬유파편 길이와 형상비는 감소하는 반면에 계면전단강도는 증가를 보였다. 함유된 섬유수가 증가함에 따라, 계면전단강도는 단계적 다섬유 복합재료에서 감소를 보여 주었다. 단계적 다섬유 복합재료는 섬유간의 거리에 의존하는 응력전달에 대한 직접적인 비교를 제공할 수 있을 것이다.

ABSTRACT: To investigate the interfacial properties depending on the inter-fiber separation among neighboring fibers, two-typed model composites were used. One is the regular- and another is the gradual multi-fiber composites. The multi-fiber fragmentation test was used to measure the interfacial shear strength (IFSS) for both specimens. According to Weibull statistical analysis, the tensile strength and the elongation for glass fiber decreased with increasing gauge length because of the size effect. For both the regular and the gradual multi-fiber composites, IFSS depended on the distance of the inter-fiber separation. As the inter-fiber separation increased, the fragment length and the aspect ratio decreased whereas IFSS increased. As the number of embedded fibers increased, IFSS decreased for the regular multi-fiber composites. The gradual multi-fiber composite can provide a direct comparison of stress transfer depending on the inter-fiber separation distance compared to the regular multi-fiber composite.

Keywords: gradual multi-fiber composites, regular multi-fiber composites, multi-fiber fragmentation test, interfacial shear strength, inter-fiber separation.

INTRODUCTION

The interfacial adhesion is an important factor to determine properties of composite materials. To evaluate the interfacial adhesion of composite materials, the micro-specimen embedded with fibers had been used using the micromechanical tests, which were to evaluate the IFSS between fiber and matrix. Some conventional techniques for IFSS include the single fiber microdroplet test,[1,2] single fiber composite (SFC) test[3-5] and microindentation test.[6]

The single microdroplet test (which is also known as the single fiber pull-out test[1,2,7]) was shown to be the best method to measure IFSS because it can directly measure interfacial adhesion between the fiber and matrix, and it is not limited by the properties of the fiber and matrix. In the SFC test (also known as the fragmentation test) the failure strain of the matrix should be several times larger than the failure strain to cause a saturated fragmentation state. In practice, however, both techniques are complementary to each other.

The SFC technique, originally proposed by Kelly-Tyson[8] for the fiber/metal composites, can provide abundant statistical informations as well as the interfacial failure modes and the IFSS using only several specimens. Based on the force balance in a micromechanical model, Kelly and Tyson showed that IFSS, τ is given by,

$$\tau = \frac{\sigma_f \cdot d}{2 \cdot \bar{l}_c} \tag{1}$$

where, d is the fiber diameter, σ_f is the fiber fracture strength, and $\bar{l}_c$ is average critical fragment length. Since the actual fragment length and the fiber strength are not constant but are strongly dependent on the gauge length, Eq. (1) can be modified by,

$$\tau = \frac{\sigma_f \cdot d}{2 \cdot \bar{l}_c} \cdot K \tag{2}$$

where, σ_f is the fiber tensile strength at a gauge length equal to the mean fragment length $\bar{l}_c$ and K is a coefficient which depends on the variation.[9] If the fragment length varies between $l_c/2$, and l_c, $K=0.75$ can be taken as a mean value. Since a distribution of fragment lengths is observed experimentally, Drzal et al.[10] altered the equation to reflect Weibull statistics to the form,

$$\tau = \frac{\sigma_f}{2 \cdot \alpha} \cdot K \tag{3}$$

$$K = \Gamma\left[1 - \frac{1}{\beta}\right] \tag{4}$$

where β is the shape parameter, α is the scale parameter in the Weibull distribution for the aspect ratio and Γ is the Gamma function.

Since SFC technique considers only an interface between fiber and matrix, it can not match well with the interfacial properties of the real composites. The model of multi-fiber composite was introduced because of the similarity with the real composites.[11-14] Regular multi-fiber composites were prepared with equal inter-fiber separation. The multi-fiber fragmentation test was used to know the fiber to fiber interaction as a function of the inter-fiber distance.

A new concept of the gradual multi-fiber composite is similar to the regular multi-fiber composites except gradually-increasing inter-fiber spacing. As the inter-fiber spacing increases gradually, the fiber to fiber interaction and IFSS depending on the distance of fiber separation were compared. The main objective is to investigate the interfacial properties among neighboring fibers with gradually increasing gaps. The comparison of IFSS and the

microfailure modes for the regular- or the gradual multi-fiber composites were evaluated using the multi-fiber fragmentation test.

EXPERIMENTAL

Materials.

Fiber: E-glass fiber with diameter of 30.3 μm was used without sizing treatment, which was supplied from Dow Corning Co. The strength of the glass fiber was measured by the tensile test using single fiber specimens. The elastic moduli and the average density of the glass fiber were 58.6 GPa and 2.55 g/cm^2, respectively. The tensile properties of the glass fiber were measured before preparing the micro-composite specimens.

Polymer Matrix: The multi-fiber composites were prepared with epoxy resin (YD-128), which was provided from Kukdo Chemical Co. Epoxy resin is based on diglycidylether of bisphenol-A (DEGBA). Jeffamine D400 and D2000 based on polyoxypropylenediamine were used as curing agents and purchased from Huntsman Petrochemical Co. Flexibility of the specimens was controlled by adjusting the relative proportions of D400 *versus* D2000 in the curing mixture for the ductile epoxy matrix. The chemical structure of curing agents is as follows:

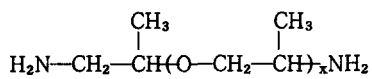

where, x is average 5.6 for D400 and 33.1 for D2000, respectively. It was precured for 2 hours at 80 ℃ and then postcured for 1 hour at 120 ℃. The m-phenlenediamine (mPDA) curing agent was also used for the comparison.

Methods.

Measurement of Single Fiber Tensile Properties: About fifty specimens in each gauge length were tested. The gauge lengths of testing specimen were 2, 5, 10, 20, and 100 mm, respectively. An average diameter of fifty glass fibers was measured by an optical microscope (Nikon model: HEX-DX) attached a calibrated eye's piece. The diameter of a fiber was measured at three different points, and the minimum value of the measured diameter was chosen.

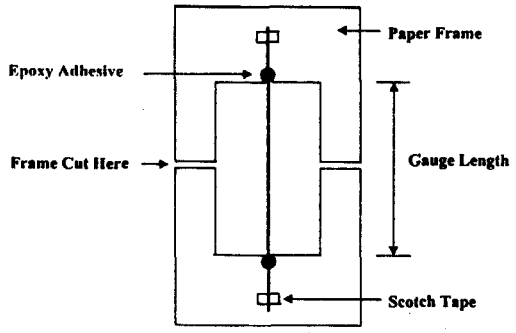

Figure 1. Paper frame and attached fiber to measure a single fiber tensile test.

A single fiber was placed on paper frame and then was fixed by Scotch tape in the center line on both ends. The epoxy adhesive was used to fix a fiber on paper frame (Fig. 1). Tensile strength was measured using the universal testing machine (Lloyd instruments Ltd Co., LR-5K) attached with 100 N load cell. The cross head speed was 0.5 mm/min.

Preparation of the Regular or the Gradual Multi-fiber Composites: The dimension of two-typed multi-fiber specimens were 3 mm wide, 25 mm gauge length, and 1 mm thickness as shown in Fig. 2(a) and (b), respectively. Space bars serving as an inter-fiber separation were equipped. After multi-fibers were laid down between space bars, the end of a fiber was fixed by Scotch tape. For the gradual multi-fiber composites, all inter-fiber spacing was the same magnitude. For the gradual multi-fiber

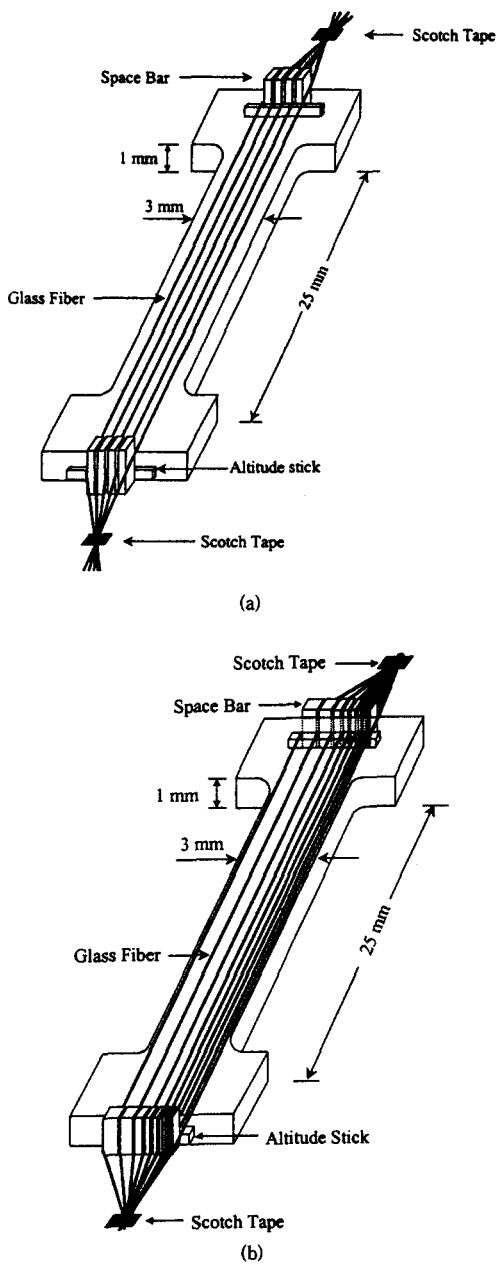

Figure 2. Schematic illustration showing the fiber arrangement and the inter-fiber separation in two-typed composites: (a) the regular multi-fiber composite; and (b) the gradual multi-fiber composite.

composites. The inter-fiber spacing, d_i increased gradually by suitably-multiple distance of fiber diameter as follows: 1 time : 30 μm ; 2 times : 60 μm ; 3 times : 90 μm ; 4 times : 120 μm ; 5 times : 130 μm ; 7 times : 210 μm ; 10 times : 300 μm ; and 15 times : 500 μm , respectively.

Multi-fibers were embedded in the flexibilized epoxy using Jeffamine curing agents on a silicon mold. After these specimens were left at room temperature for 24 hours, they were precured at 80 ℃ for 2 hours and postcured at 120 ℃ for 1 hour.

After the fiber position and the straightness were checked carefully with an optical microscope, the unsuitable specimens were discarded. After the specimen was taken out from the mold, the specimen was polished by the standard metallographic technique to obtain the smooth surface and same thickness. Bulk epoxy specimens were tested tensilely by universal testing machine (5 KN load cell, 1 mm/min crosshead speed rate). A set consisting of three specimens was tested and the stress *versus* the strain curve was drawn.

For preparing the multi-fiber composites, the degassed resin mixture was cast into a silicon mold. Each fiber was positioned at a half depth of the specimen thickness. After curing, the specimens were transparent enough to observe the microfailure modes. The specimens were tested after aging for 3 days at room temperature and humidity to equilibrate.

IFSS Measurement: IFSS of the multi-fiber composites was investigated by the multi-fiber fragmentation test. The interfacial failure occurring on the individual fiber was observed via an optical microscope with a specially-designed tensile machine. During testing, the specimen was stressed incrementally and the fibers were fractured into small segments within matrix. As the tensile stress was applied further, the fracture process continued until no longer fracture occurred in the fiber. At this strain a fragment

length is called as a critical fragment length, l_c. The critical fragment length of the individual fiber was measured and their microfailure mode was observed via a polarized-light microscope.

The classical relationship among the fiber tensile strength, the critical fragment length to diameter ratio (i.e., aspect ratio, l_c/d) and IFSS, τ was given by Kelly-Tyson as in the Eq. (1). Widely-distributed τ values are obtained as a result of the random distribution and the heterogeneity of the flaws in fibers. The data for the both fragment length and the fiber strength may be approximated by Weibull distribution[15] and these distributions can be combined to calculate IFSS. The cumulative probability of failure of a fiber length l loaded to stress level σ is given by,[16]

$$F = 1 - \exp\left[-l\left(\frac{\sigma}{\sigma_0}\right)^m\right] \tag{6}$$

where σ_0 is the scale parameter, m is the shape parameter (or Weibull modulus), the mean value of the estimated probability, and F is assigned as,

$$F = \frac{i}{N+1} \tag{7}$$

where N is the total number of the fiber fragments, and i is the rank number. To evaluate the parameters, m and σ_0, Eq. (6) can be rearranged into a linearized form as,

$$\ln[-\ln(1-F)] = \beta \ln(t) - \beta \ln \alpha \tag{8}$$

Thus, a plot of ln [-ln (1-F)] *versus* ln (aspect ratio) yields a straight line which slope and intercept yields β and α, respectively. IFSS can be calculated by previous Eq. (3).

To know the tensile strength at the critical length, a direct tensile test at such a short length can result in experimental difficulties. Fiber strengths are usually determined by the macroscopic gauge lengths, and then with subsequent extrapolation to smaller gauge length using Weibull weakest link rule.[17] It was calculated from the extrapolation of the fiber strength measured at a individual gauge length. The fiber strength at the critical fragment length is

$$\sigma_f = \sigma_0 \cdot \left(\frac{l_c}{l_0}\right)^{-\frac{1}{m}} \tag{9}$$

where, σ_0 is fiber strength at gauge length, l_0 and m is the shape parameter of Weibull distribution for fiber strength.[18]

RESULTS AND DISCUSSION

Statistical and Mechanical Analysis of Fiber and Matrix. Tensile strength of most ceramic fibers such as glass fiber is known to be dependent on the gauge length due to the probability of flaws along the fiber surface. Table 1 shows the tensile strength and elongation of single glass fiber depending on various gauge lengths. As the gauge length increased, both the tensile strength and the elongation decreased. It was due to the existence of defects and the heterogeneous distribution of flaws, which existed either on the fiber surface or internally. Fig. 3 shows Weibull parameters of the glass fiber with gauge length from Weibull statistical analysis. As gauge length decreased, the shape parameter increased due to less propability of defects.

Table 2 shows the tensile properties of epoxy specimen with various curing agents and their stress-strain curve is shown in Fig. 4. Epoxy (a) using mPDA hardener was the most rigid and brittle with the highest tensile strength, modu-

Table 1. Values of Tensile Properties and Their Weibull Parameters of Glass Fiber (Diameter 30.3 μm) with Various Gauge Lengths

gauge length (mm)	no. of specimen (EA)	diameter (μm)	elongation (%)	tensile strength (MPa)	scale parameter (α)	shape parameter (β)
2	40	0.3 (1.7)[a]	11.4 (2.5)	2487	2619	5.1
5	44	30.1 (1.1)	5.7 (1.2)	2206	2483	4.1
10	45	30.3 (1.3)	4.9 (1.4)	1956	2031	4.3
20	37	30.1 (1.0)	2.8 (0.9)	1483	1803	3.7
100	42	30.6 (2.0)	1.4 (0.4)	1029	1215	3.8

[a] Standard deviation.
* Used estimator is $F(X_i)=i/(N+1)$.

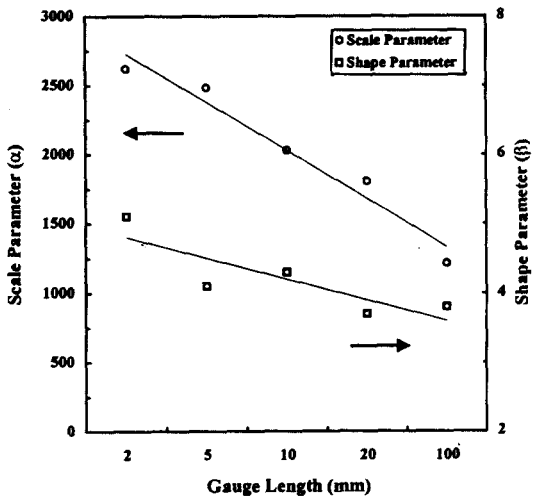

Figure 3. Scale and shape parameters of glass fibers (30.3 μm diameter) with various gauge lengths.

lus and the smallest elongation. As the amount of the flexible curing agent increased, tensile modulus decreased whereas elongation increased. Epoxy (c) and (d) showed more ductile with higher elongation and the uniform deformation without necking. Epoxy (c) showed higher tensile modulus than epoxy (d). At highly-elongated range epoxy (d) showed slightly increasing trend because of the strain hardening. Due to the multi-fibers embedded in epoxy matrix, sufficient ductility is necessary to get enough elongation for giving the

Table 2. Mechanical Properties of the Epoxy Specimens with Various Curing Agents

curing agent	tensile stdrength (MPa)	modulus (GPa)	strain of breakage (%)
mPDA	84.2 (7.0)[a]	2.52 (0.4)	5.5 (0.8)
D400	41.4 (3.8)	2.00 (0.2)	8.8 (2.6)
D400+D2000	35.8 (6.6)	1.76 (0.2)	40.5 (3.8)
D400+D2000	24.6 (1.9)	1.56 (0.2)	66.6 (5.2)

[a] Standard deviation.
- mPDA : Brittle resin.
- D400, D2000 : Modified and flexible resins.
- Each four specimens were used.

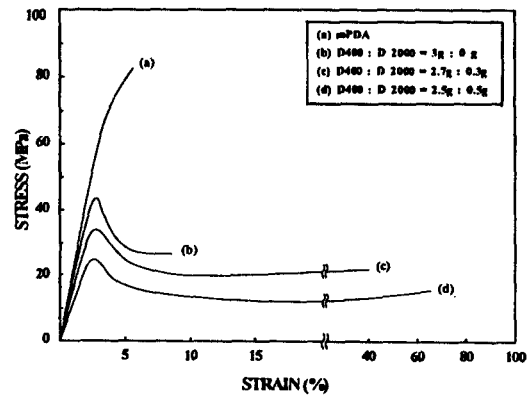

Figure 4. Plot of stress-strain curve for the dogbone-shaped epoxy specimens using four different curing agents : (a) mPDA ; (b) D2000 : 0 g ; (c) D2000 : 0.3 g ; (d) D2000 : 0.5 g.

saturated fiber fracture along the multi-fibers while straining. Epoxy (c) formula was chosen for preparaing the multi-fiber composites suitably.

Microfailure Modes in the Regular and the Gradual Multi-fiber Composites: Basic models of two different specimens are shown in Fig. 5. Fig. 5(a) to (c) represents the single- or the regular multi-fiber composites with three or five fibers, where all inter-fiber spacing was the same magnitude. The gradual multi-fiber composite was also shown in Fig. 5(d). The inter-fiber spacing, d_i increased gradually by suitably-multiple distance of fiber diameter.

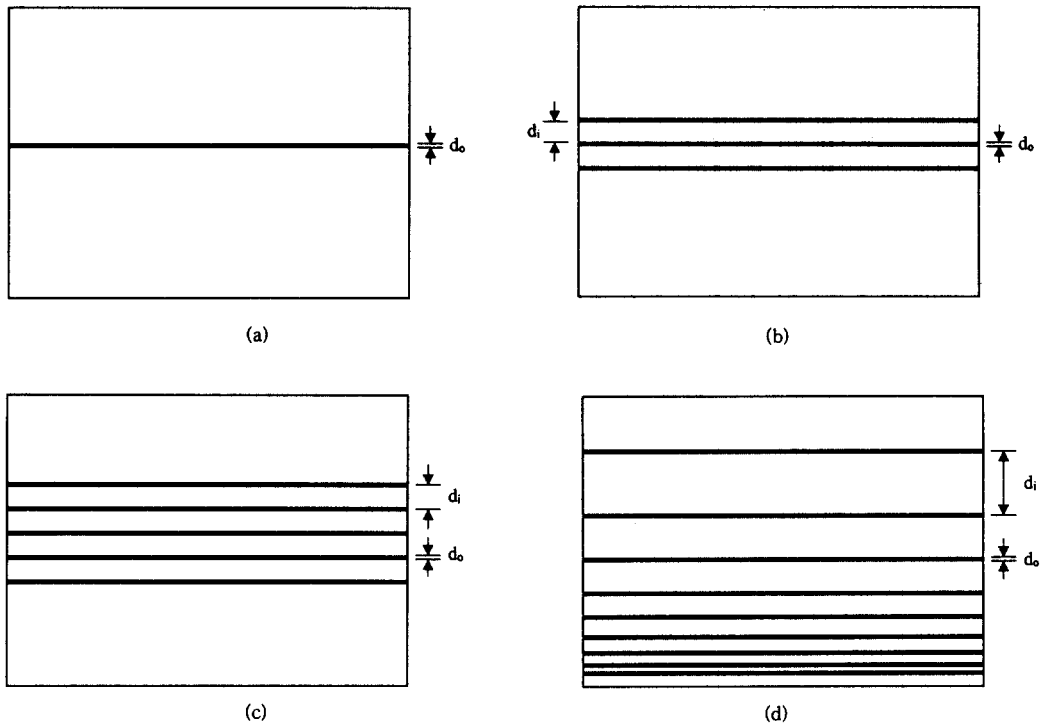

Figure 5. Dimension of specimens for the single-fiber or the multi-fiber fragmentation test : (a) single-fiber ; (b) regular three-fibers ; (c) regular five-fibers ; (d) gradual multi-fiber reinforced composites.

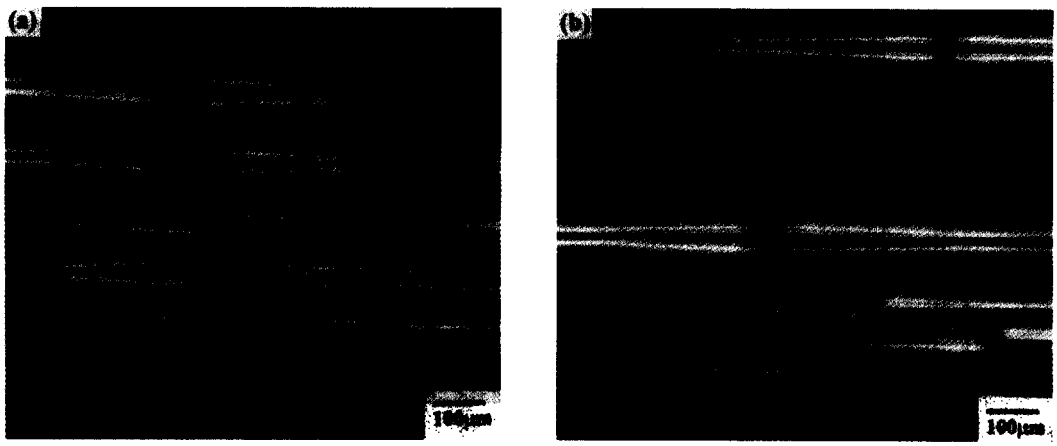

Figure 6. Optical photographs of the fiber fractures in multi-fiber composites with a polarized-light : (a) the regular- ; (b) the gradual multi-fiber composites.

Fig. 6 shows the shear stress birefringence in the matrix around the break in (a) the regular- and (b) the gradual multi-fiber composite with a polarized-light. In Fig. 6(a), distinct fiber fracture modes were exhibited and all fibers were broken successively in a series around neighbor-

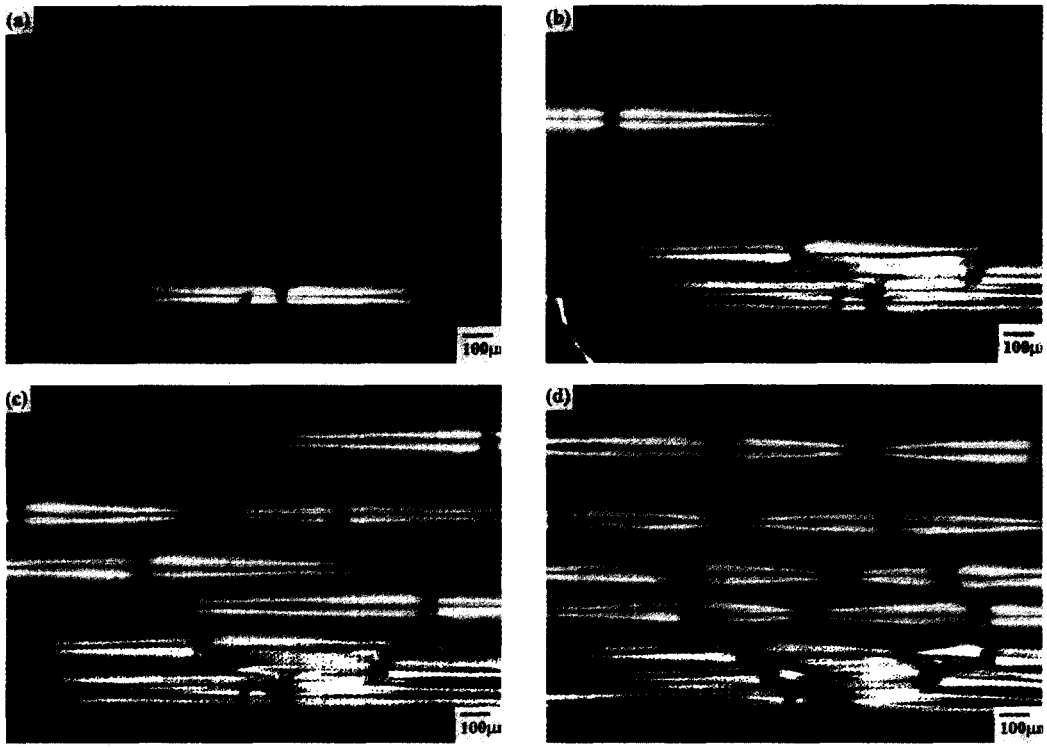

Figure 7. A series of photographs with increasing of the tensile strain: (a) 1% strain; (b) 4% strain; (c) 6% strain; (d) 10% strain.

ing fibers. It was considered because the fracture energy of a fiber affected adjacent fibers. The breaking trend in a series was observed in a whole gauge range of testing specimens. In Fig. 6(b), however, breaking positions in the individual fiber were rather random or irregular.

Fig. 7 shows a series of the birefringence pattern of the fiber failure modes in the gradual multi-fiber composite. When the tensile stress was applied, a fiber break occurred at a position of the narrow fiber in the initial stage. It could be because higher stress concentration can exist around the narrow multi-fibers compared to that of the wider multi-fibers. At a breaking position, stress whitening was observed with high angle. This angle became lower while further tensile loading. Two matrix cracks at close two fibers were overlapped and the cone-shaped crack was propagated to perpendicular direction of the fiber axis. Crack gap increased further with an increase of elongation. One of the significantly-large crack cone may result in a catastrophic failure of specimen at high elongation.

By appling tensile stress, more fiber breaks at the wide fiber occurred. The number of fiber breaks at the wide fiber was larger than that of the narrow fiber. Fiber fracture energy transferred from a position of the broken fiber to an another weak position along the same fiber axis.

IFSS of Two-typed Multi-fiber Composites: The interfacial properties of the SFC and regular multi-fiber composites using the multi-fiber fragmentation test are given in Table 3. Fig. 8 shows the average aspect ratio and their

Table 3. Values of the Interfacial Properties Using the Single-fiber and the Regular Multi-Fiber fragmentation Test

interfacial properties	no. of embedded Fibers						
	1(EA)	3(EA)			5(EA)		
fiber separation, d_i/d_o[a]	–	2.0	3.4	5.1	1.7	4.0	4.9
ave. fragment length (mm)	0.85	1.0	0.9	0.9	1.0	1.0	0.9
ave. aspect ratio	27.9	32.8	31.0	29.9	34.4	31.4	31.3
IFSS (MPa)	49.5	40.8	44.2	45.8	38.6	43.1	43.6

[a] d_i and d_o are inter-fiber spacing and fiber diameter, respectively.

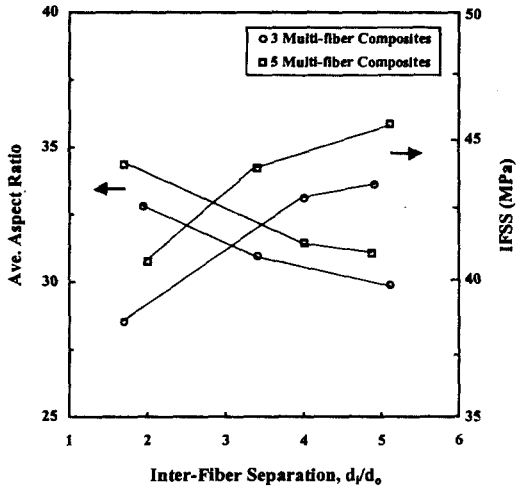

Figure 8. Effect of the inter-fiber separation on the average aspect ratio and IFSS in the regular three- or five-fiber composites.

IFSS with inter-fiber separation in three and five multi-fiber composites. The inter-fiber spacing is an important factor to determine the interfacial adhesion in the model composites. As the inter-fiber separation became wider, mean fragment length and aspect ratio decreased whereas IFSS increased. In the narrow separation, the fracture energy of a fiber break can affect the adjacent fiber just upper or below.

Fig. 9 shows the change of IFSS depending on the number of embedded fiber in the SFC and multi-fiber composites. The more number of embedded fibers, the lower the IFSS. Because multi-fiber composites can contain multiple failure bundle which causes the crack propagation and results in a catastrophic failure of the specimen. Especially, SFC showed considerably-higher IFSS compared to that of multi-fiber composites. It may be because the SFC can extend higher elongation until fracture occurred due to the absence of multiple-bundle failure. In addition, there is no stress dissipation toward adjacent fibers.

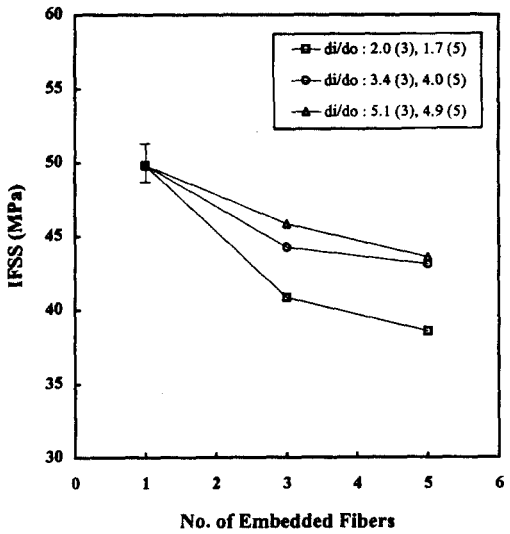

Figure 9. IFSS as a function of the number of embedded fibers in the single-fiber and the regular multi-fiber composites.

The interfacial properties of the gradual multi-fiber composites using multi-fiber fragmentation test is given in Table 4. Fig. 10 shows (a) the average aspect ratio and (b) IFSS with an increase of inter-fiber separation in the gradual multi-fiber composite. Nine fibers were embedded in epoxy matrix gradually. As the distance of the inter-fiber separation increased, average fragment length and their aspect ratio decreased continuously whereas IFSS increased almost linearly for both 6 and 12% elongation.

After a fiber was broken, next fiber breakage did not occur along the same fiber axis, but oc-

Table 4. Values of the Interfacial Properties Using the Gradual Multi-fiber Fragmentation Test

order of fibers		1	2	3	4	5	6	7	8	9
elongation	fiber separation (d_i/d_o)[a]	0.9	0.8	1.9	4.0	4.3	7.1	8.9	15.7	-
6%	fragment length (mm)	1.4	1.5	1.4	1.4	1.3	1.3	1.2	1.1	1.1
		(0.3)[b]	(0.4)	(0.2)	(0.2)	(0.3)	(0.2)	(0.1)	(0.2)	(0.1)
	aspect ratio	42.1	49.4	46.4	44.5	42.8	45.9	39.7	36.9	37.5
		(9.3)	(12.9)	(7.2)	(5.2)	(8.6)	(5.4)	(3.2)	(6.3)	(4.4)
	IFSS (MPa)	28.8	26.7	27.6	28.6	30.6	29.4	32.6	36.2	35.2
		(6.8)	(9.2)	(5.7)	(4.0)	(7.0)	(4.7)	(3.3)	(6.7)	(5.3)
12%	fragment length (mm)	1.2	1.3	1.4	1.3	1.3	1.2	1.1	1.0	1.0.
		(0.1)	(0.2)	(0.1)	(0.1)	(0.2)	(0.2)	(0.1)	(0.2)	(0.1)
	aspect ratio	39.4	40.2	42.5	41.4	41.1	38.1	36.3	33.5	33.2
		(1.8)	(6.5)	(4.0)	(3.1)	(6.18)	(7.5)	(3.3)	(6.0)	(2.8)
	IFSS (MPa)	32.7	32.6	31.1	31.4	31.6	35.3	36.4	40.8	40.4
		(1.8)	(5.7)	(3.5)	(2.0)	(5.6)	(8.2)	(3.9)	(8.5)	(3.9)

[a] d_i and d_o are inter-fiber spacing and fiber diameter, respectively, [b] Standard deviation (SD).
* Glass fiber diameter : 30.3 μm.

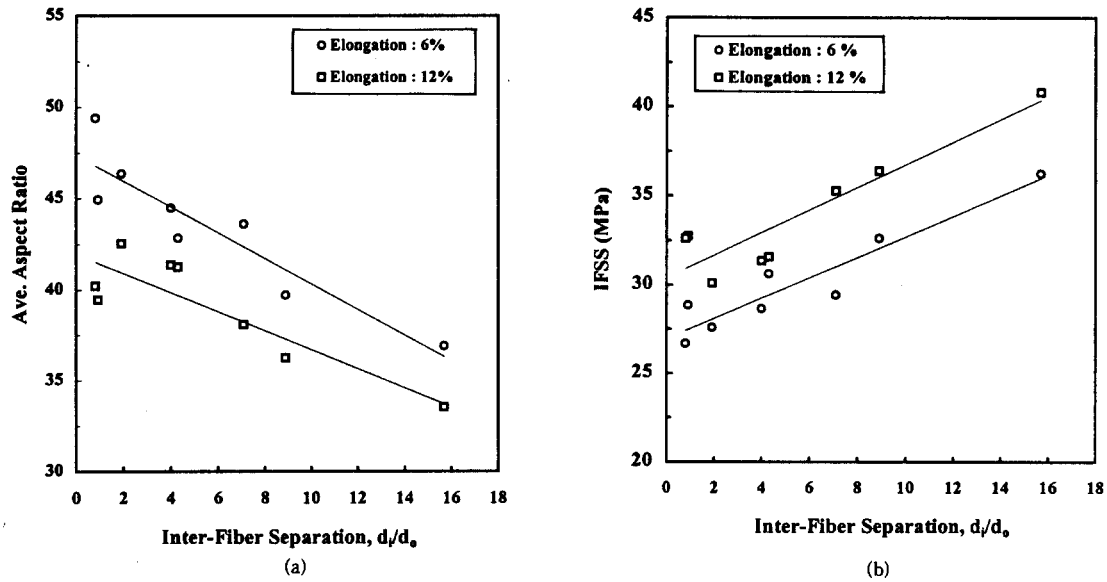

Figure 10. (a) The average aspect ratio and (b) IFSS as a function of the inter-fiber separation at 6% and 12% elongations.

curred at a weak section of adjacent fibers. The fiber usually started to break at narrow sections, and then propagated toward wider sections. In the narrow section, breaking positions were similar comparing with those at upper and below fibers. In the initial stage the number of fiber breakage was larger in the narrow fibers. As the strain increased further, the number of the fiber breakage became larger in the wider section. In the narrow section, many failures exhibited the continuous steps-like shape with further straining. In the narrow inter-fiber separation, the

stress occurred from a fiber breakage and subsequent matrix crack seems to affect neighboring fibers breakage rather than another failure along the same fiber axis. Neighboring fibers may absorb the dissipated energy from a fiber breakage. This overlapped failure portion resulted in the total failure in the specimen during the testing.

As a main advantage, gradual multi-fiber composite can provide the direct comparison of stress transfer depending on the inter-fiber separation compared to the regular multi-fiber composite. It also can save a tedious testing time with identical testing conditions, such as matrix, loading etc. Since the inter-fiber separation may not be same distance in real composites, gradual multi-fiber model composite can be considered as *in-situ* composites.

CONCLUSIONS

The interfacial properties of the regular and gradual multi-fiber composites were compared by using multi-fiber fragmentation test. According to Weibull statistical analysis, tensile strength and elongation for glass fibers decreased with increasing gauge length because of the size effect based on surface flaws. From both regular- or gradual multi-fiber composites, IFSS depended on the distance of the inter-fiber separation. As the inter-fiber separation increased, the fragment length and the aspect ratio decreased whereas IFSS increased. It was considered because the stress was preferentially transferred from a broken fiber to the neighboring fibers rather than to another weak position along the same fiber axis. As the number of embedded fiber increased, IFSS decreased in the regular multi-fiber composites. The gradual multi-fiber composite can provide a direct comparison of stress transfer depending on the inter-fiber separation distance.

Acknowledgement: This work was financially supported by Regional Research Center for Aircraft Parts Technology (ReCAPT) of KOSEF.

REFERENCES

1. A. R. Sanadi and M. R. Piggott, *J. Mater. Sci.*, **20**, 431 (1985).
2. J. M. Park and S. I. Lee, *Polymer (Korea)*, **21**(4), 689 (1997).
3. J. M. Park, R. V. Subramanian, and A. E. Bayoumi, *J. Adhesion Sci. Technol.*, **8**, 133 (1994).
4. J. M. Park, J. O. Lee, and T. W. Park, *Polym. Compo.*, **17**, 375 (1996).
5. J. M. Park and R. V. Subramanian, *J. Adhesion Sci. Technol.*, **5**, 459 (1991).
6. D. B. Marshall and W. C. Oliver, *Mater. Sci. Eng.*, **A126**, 95 (1990).
7. T. Grubb and Z. F. Li, *J. Mater. Sci.*, **29**, 189 (1994).
8. A. Kelly and W. R. Tyson, *J. Mech. Phys. Solids*, **13**, 329 (1965).
9. A. S. Wimolkiatisak and J. P. Bell, *Polym. Compo.*, **10**, 162 (1989).
10. L. T. Drzal, M. J. Rich, M. F. Koenig, and P. F. Lloyd, *J. Adhesion*, **16**, 133 (1983).
11. Z. F. Li, D. T. Grubb, and L. Phoenix, *Compos. Sci. Technol.*, **54**, 251 (1995).
12. J. K. Kim and Y. W. Mai, *J. Mater. Sci.*, **30**, 3024 (1995).
13. M. L. Accorsi, A. Pegoretti, and A. T. Dibenedetto, *J. Mater. Sci.*, **31**, 4181 (1996).
14. P. W. J. Van Den Heuvel, T. Peijs, and R. J. Young, *J. Mater. Sci. Lett.*, **15**, 1908 (1996).
15. W. Weibull, *J. Appl. Phys.*, **18**, 293 (1951).
16. S. N. Patankar, *J. Mater. Sci. Lett.*, **10**, 1176 (1991).
17. H. F. Wu and A. N. Netravali, *J. Mater. Sci.*, **27**, 3318 (1992).
18. K. Goda, J. M. Park, and A. N. Netravali, *J. Mater. Sci.*, **30**, 2722 (1995).